Astronomy & Astrophysics manuscript no. paperabund
(DOI: will be inserted by hand later)

June 25, 2004

Coronal versus photospheric abundances of stars with different activity levels*

J. Sanz-Forcada[1], F. Favata[2], and G. Micela[1]

[1] INAF – Osservatorio Astronomico di Palermo G. S. Vaiana, Piazza del Parlamento, 1; Palermo, I-90134, Italy
[2] Astrophysics Division – Research and Science Support Department of ESA, ESTEC, Postbus 299, NL-2200 AG Noordwijk, The Netherlands

Received 7 October 2003 / Accepted 6 November 2003

Abstract. We report a detailed analysis of the coronal abundance of 4 stars with varying levels of activity and with accurately known photospheric abundances. The coronal abundance is determined here using a line flux analysis and a full determination of the differential emission measure. Photospheric abundance values are taken from the literature. Previous coronal abundance determinations have generally been compared to solar photospheric abundances; from this a number of general properties have been inferred, such as the presence of a coronal metal depletion with an inverse First Ionization Potential correlated with activity level. Here we show that, when coronal abundances are compared with real photospheric values for the individual stars, the resulting pattern can be very different. Also, we present evidence that, in some cases, the coronal metal abundance may not be uniform in the corona; in particular it can vary with the temperature of the emitting plasma.

Key words. stars: coronae – stars: abundances – stars: late-type – x-rays: stars – Line: identification

1. Introduction

Following the initial results from the ASCA-SIS instrument (e.g. White et al., 1994; Drake, 1996), which showed that the low-resolution X-ray spectra of active coronal sources were often best fit with a low metal abundance (typically about 0.3 the solar photospheric abundance), the issue of the metal abundance of the coronal plasma has become one of the main areas of interest for X-ray spectroscopy of active stars. Due to the limited spectral resolution of the ASCA spectra, the determination of abundance for elements other than Fe was often not accurate (Favata & Micela, 2003). The availability of the XMM-*Newton* and *Chandra* high-resolution X-ray spectra of coronal sources has allowed observing individual, resolved spectral lines of a number of elements in the corona of active stars, and thus to address the issue of the abundance of a number of elements. Unfortunately up to now the results have not been as conclusive as initially expected. One reason is that often the same data analyzed with different approaches result in significantly different values for the element abundances (see Favata & Micela, 2003, for a number of examples).

One of the issues most often addressed by coronal abundance studies is whether a bias of the First Ionization Potential (FIP) of the element is present. Such an "FIP effect" is found in the solar corona, where the abundance of elements with low FIP (< 10 eV; e.g. Mg, Si, Fe) is observed to be enhanced with respect to their photospheric values, while elements with high FIP ($\gtrsim$ 10 eV; e.g. O, Ne, Ar) remain at abundances similar to the photospheric values. Such a behavior is observed in the upper solar atmosphere at temperatures higher than $\sim$ 1 MK, both in the non-active regions and in full-disk spectra (Laming et al., 1995; Feldman & Laming, 2000). EUVE observations showed the same FIP bias to be present in stars with low activity levels, such as α Cen AB (G2V+K1V, Drake et al., 1997), and possibly (only limited knowledge of their photospheric abundance was available at that time) ξ Boo A (G8V, Laming & Drake, 1999) and ϵ Eri (K2V, Laming et al., 1996). EUVE spectra of more active stars did not show any FIP effect, with however a rather low coronal Fe abundance with respect to the solar photosphere, which suggested some metal depletion in the corona of the active stars. Feldman & Laming (2000) review some of the results on solar and stellar coronal abundances previous to *Chandra* and XMM-*Newton*.

The new generation of X-ray satellites XMM-*Newton* and *Chandra* offers access to high resolution spectra in a wavelength region where numerous spectral lines from different elements are formed at coronal temperatures. This permits one to measure the fluxes of individual lines, in principle allowing a much better determination of the coronal thermal structure and abundances. Initial results on coronal abundances determined from data from the two observatories have been reviewed by

Send offprint requests to: J. Sanz-Forcada, e-mail: `jsanz@astropa.unipa.it`

* Tables 4–7 are only available in electronic form at the CDS via anonymous ftp to cdsarc.u-strasbg.fr (130.79.128.5) or via http://cdsweb.u-strasbg.fr/cgi-bin/qcat?J/A+A/

Table 1. Observation log

Object	HD #	SpT	Instrument	$\lambda\lambda$(Å)	$t_{\rm exp}$ (ks)	Date	d (pc)	$L_{\rm X}$	$L_{\rm X}/L_{\rm bol}$	$L'_{\rm X}$
Procyon	61421	F5IV	*Chandra*/LETG	3–175	69.6	6 Nov 1999	3.50	8.89E27	3.39E-7	9.41E26
Procyon	61421	F5IV	*Chandra*/LETG	3–175	69.7	7 Nov 1999	"	"	"	"
ϵ Eri	22049	K2V	*Chandra*/LETG	3–175	105.3	21 Mar 2001	3.22	1.79E28	1.42E-5	9.65E27
λ And	222107	G8III/?	*Chandra*/HETG	1.7–27	81.9	17 Dec 1999	25.8	2.74E30	3.25E-5	1.73E30
V851 Cen	119285	K2IV-III/?	XMM/RGS	4–38	29.2	7 Mar 2003	76.2	6.46E30	3.01E-4	4.47E30

Note: Distances (d) from Perryman et al. (1997). $L_{\rm X}$ (erg s^{-1}) in the range 5–100 Å (0.12–2.4 keV), the range covered by the ROSAT/PSPC. $L'_{\rm X}$ (erg s^{-1}) in the range 6–20 Å (0.62–2.1 keV), common to RGS, HETGS and LETGS.

Drake (2002) and Favata & Micela (2003). These new results seem to point towards a scenario with stars with low activity levels showing, when their coronal and photospheric abundances are compared, a solar-like FIP effect (case of α Cen, Raassen et al., 2003) or no FIP bias (for Procyon, Raassen et al., 2002). Active stars (like HR 1099, II Peg, AR Lac or AB Dor), with a quite different coronal thermal structure, dominated by material emitting at temperatures of $\sim$ 10 MK, show a pattern characterized by a general depletion of elements with low FIP (when they are compared with solar photospheric values) while the elements with high FIP remain at solar (or sometimes higher) photospheric values (Drake et al., 2001; Brinkman et al., 2001; Huenemoerder et al., 2001, 2003; Sanz-Forcada et al., 2003b) although photospheric abundances of elements other than Fe are not known for HR 1099. Audard et al. (2003) analyzed XMM-*Newton* observations of 5 active binary systems, concluding that low-FIP elements are subject to greater depletion in more active stars, while high-FIP elements remain at similar levels (although photospheric abundances were available only for one of the objects in their sample, namely λ And). In general, the comparison of stellar coronal abundances with solar photospheric values is of little use, given the wide range of abundances found among late type stars (e.g. Cayrel de Strobel et al., 2001). Most of the stars for which coronal abundances have been determined have no published photospheric abundances, so that a true test of FIP-related effects cannot be done. This is especially true for active stars, for which the large rotational velocity complicates the measurements of photospheric abundances. In most cases the available photospheric abundances are limited to Fe (e.g. Randich et al., 1993), and even these in many cases are likely to be affected by systematic errors. Moreover, different methods to determine the distribution of material with temperature in the corona (the so called "emission measure distribution", EMD) sometimes produce contradictory results, depending on the analysis technique employed (Favata & Micela, 2003; Sanz-Forcada et al., 2003b).

In the present work we determine the coronal thermal structure and abundances of four stars with different activity levels (in terms of $L_{\rm X}/L_{\rm bol}$) observed with relatively high statistics with *Chandra* and XMM-*Newton* (see Table 1), and for which there are accurate photospheric abundance measurements available, to explore the relation between activity levels and coronal relative abundance patterns. The chosen stars are Procyon (one of the stars with lowest $L_{\rm X}/L_{\rm bol}$ values), the intermediate activity star ϵ Eri, the long-period active binary λ And and the active binary V851 Cen. These four objects are among the few stars for which both high-resolution coronal spectra with good statistics and measurements of photospheric abundances for several elements are available.

The observations are described in Sect. 2, a brief description of the analysis techniques is presented in Sect. 3. The results for each star are discussed in Sect. 4, followed by the discussion and conclusions in Sect. 5.

2. Observations

We have analyzed observations conducted using different X-ray high-resolution spectrographs; however, the spectral lines observed in the different spectra are formed in very similar temperature ranges ($\log T$[K] $\sim$ 5.5–7.8), hence yielding information of the same region of the corona (see Sect. 3). The X-ray luminosity of the targets has been calculated by modeling the observed spectra, as listed in Table 1.

2.1. V851 Cen

An XMM-*Newton* observation of V851 Cen (P.I. F. Favata) was executed in March 2003 (Table 1). XMM-*Newton* carries out simultaneous observation with the EPIC (European Imaging Photon Camera) PN and MOS detectors (sensitivity range 0.15–15 keV and 0.2–10 keV respectively), and with the RGS (Reflection Grating Spectrometer, den Herder et al., 2001) ($\lambda\lambda$ ~6–38 Å, $\lambda/\Delta\lambda$ ~100–500). The RGS data have been reduced employing the standard SAS (Science Analysis Software) version 5.4.1 package, removing in the RGS spectra the time intervals when the background was higher than 0.4 cts/s in CCD #9, to ensure a "clean" spectrum. Light curves were obtained by selecting a circle centered on the source in the EPIC-pn and EPIC-MOS images, and subtracting the background count rate taken from a nearby area. The light curve shows a slow decline ($\sim$ 20%) of the source flux (Fig. 1). High resolution spectra corresponding to the first and second orders of the RGS have been used to measure the line fluxes simultaneously, improving the quality of the measurements. Fluxes measured for second order lines are in good agreement with those in the first order (Sanz-Forcada et al., 2003b), hence they can be used to improve the quality of the measurements due to their better spectral resolution.

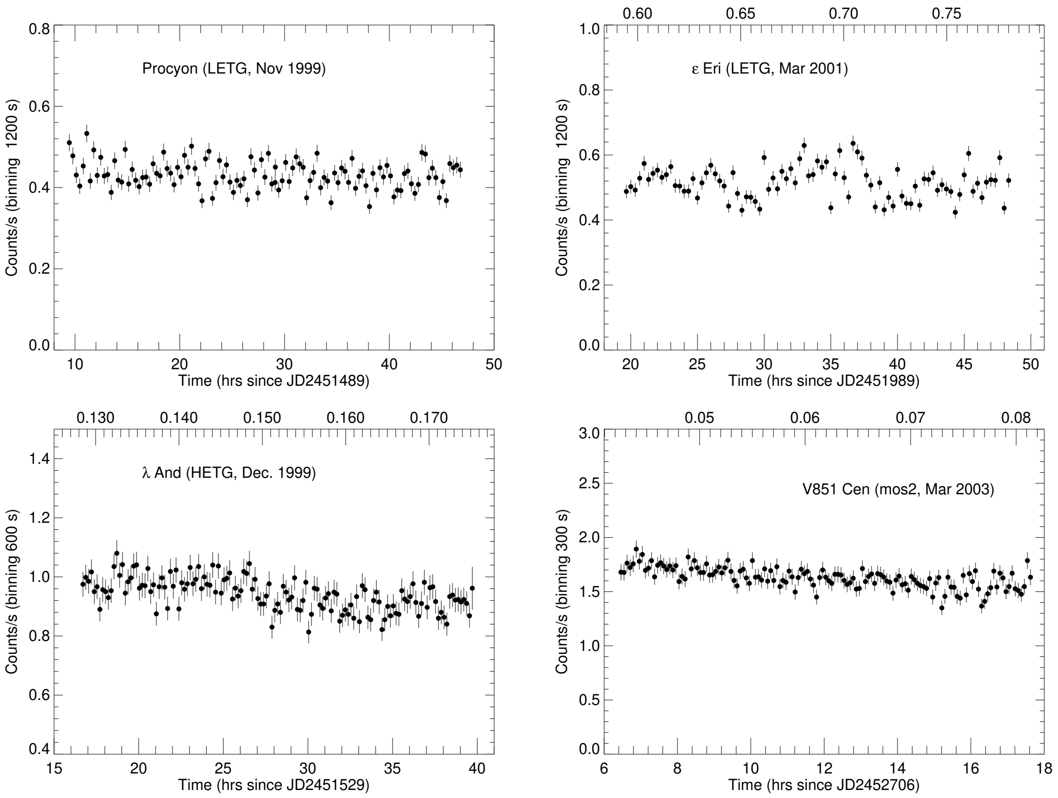

Fig. 1. Light curves of Procyon (LETGS), ϵ Eri (LETGS), λ And (HETGS) and V851 Cen (XMM/MOS 2) with 1-σ error bars. The upper axis reports the photometric phase (ϵ Eri) and orbital phase (λ And and V851 Cen, with T_0 corresponding to secondary star located behind the primary star).

2.2. λ And

An observation with the *Chandra* High Energy Transmission Grating Spectrograph (HETG, Weisskopf et al., 2002) of λ And was retrieved from the *Chandra* archive (Table 1). The HETGS is made of two gratings, HEG (High Energy Grating, $\lambda\lambda$ ~1.7–15, $\lambda/\Delta\lambda$ ~65–1070), and MEG (Medium Energy Grating $\lambda\lambda$ ~3–27, $\lambda/\Delta\lambda$ ~80–970) operating simultaneously. Standard reduction tasks from the CIAO v2.3 package have been employed in the reduction of data and the extraction of the HEG and MEG spectra. The light curve of λ And, obtained from the MEG and HEG first order spectra, shows no significant events, with variations of less than 20% of the total flux (Fig. 1).

2.3. Procyon and ϵ Eri

Observations with the *Chandra* Low Energy Transmission Grating Spectrograph (LETGS, $\lambda\lambda$ ~3–175, $\lambda/\Delta\lambda$ ~60-1000 Weisskopf et al., 2002) and the High Resolution Camera (HRC-S) of Procyon and ϵ Eri were retrieved from the *Chandra* archive as listed in Table 1. Data were reduced using standard reduction tasks present in the CIAO v2.3 package. The positive and negative spectral orders were summed for the flux measurements, although at long wavelengths ($\gtrsim$ 40 Å) separate measurements were made in the plus and minus spectra due to problems with wavelength calibration or detector gaps. Lines formed in the first dispersion order but contaminated with contribution from higher dispersion orders were not employed in the analysis. The two observations available for Procyon were summed to achieve better statistics, resulting in an exposure time of 139 ks. Light curves were obtained from the LEG spectra (first and higher orders) of Procyon and ϵ Eri as shown in Fig. 1.

3. Data analysis

X-ray spectra from stellar coronae have numerous lines from different elements formed at different temperatures. This variety of temperatures in the lines formation makes it necessary to determine in detail the thermal structure of the target star, commonly parameterized through the emission measure distribution (EMD) as a function of temperature, defined as $EM(T) = \int_{\Delta T} N_H N_e dV$ [cm^{-3}]. In the present work we apply a line-based method to reconstruct the EMD of the stellar coronae (this method is preferred to the global fitting techniques, see Sanz-Forcada et al., 2003b), with a step in temperature of 0.1 dex, the same as employed in the Astrophysical Plasma Emission Database (APED v1.3, Smith et al., 2001), which is used for comparison of the observed with the predicted line fluxes as explained below.

The EMD reconstruction was conducted by measuring the fluxes from spectral lines present in the high resolution X-ray spectra, following Sanz-Forcada et al. (2003b). The *Interactive Spectral Interpretation System* (ISIS, Houck & Denicola, 2000)

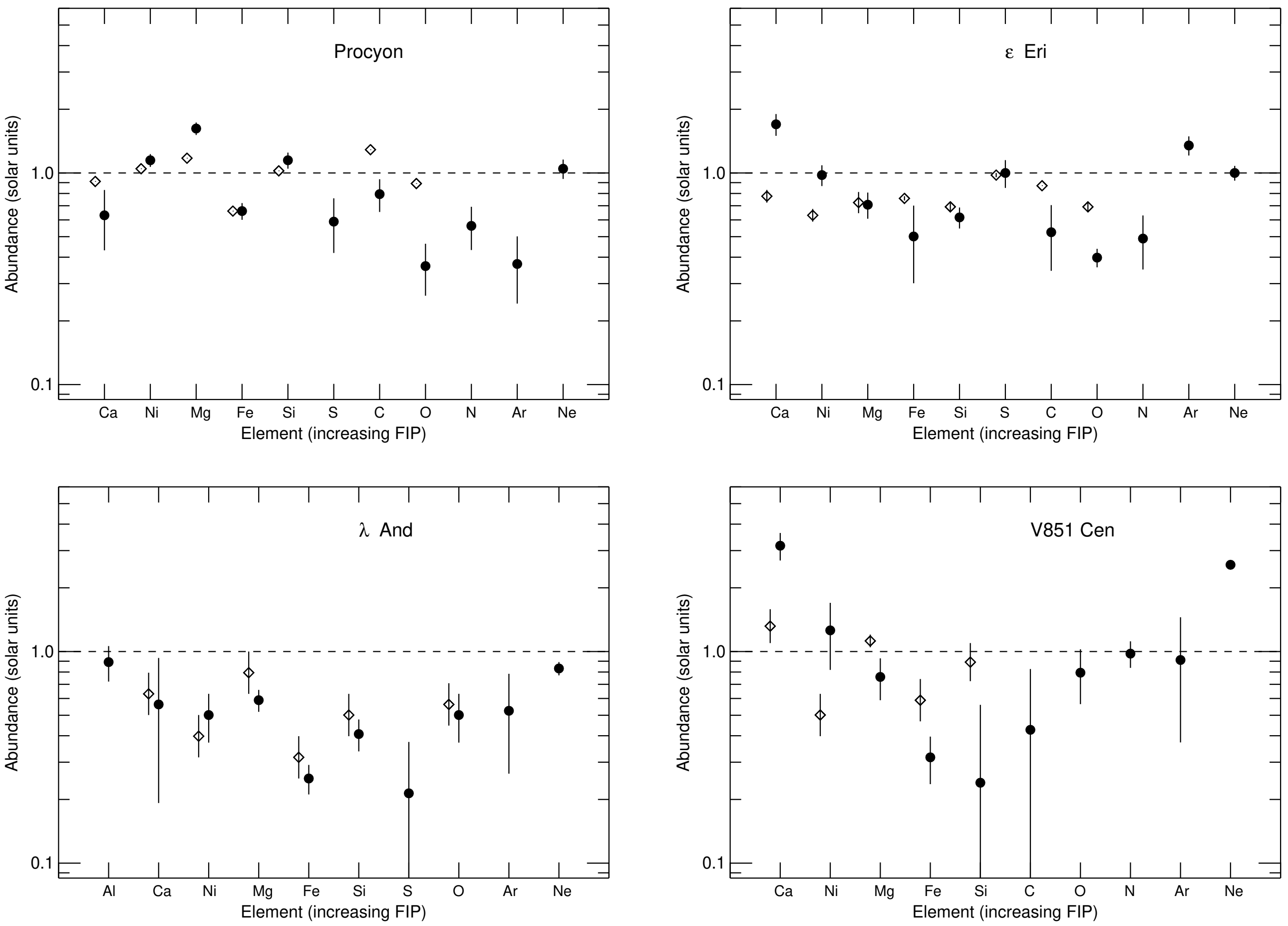

Fig. 2. Element abundances in the corona of Procyon, ϵ Eri, λ And and V851 Cen (filled circles) with respect to solar photospheric values. Open diamonds represent the stellar photospheric abundances (see text). A dashed line indicates the adopted solar photospheric abundance (Anders & Grevesse, 1989).

software package, provided by the MIT/CXC, was employed to measure the line fluxes, through convolution of the spectral response. These measured line fluxes were then corrected for interstellar medium absorption (ISM) (although such correction is important only for very few lines). Theoretical fluxes can be predicted by assuming an initial EMD which is combined with the emissivity functions of the different spectral lines. These fluxes are then compared with the observed fluxes, and the EMD is changed to determine a solution that shows a better agreement between predicted and observed fluxes. An iterative process, as explained in Sanz-Forcada et al. (2003b), results in the "best" solution for both the EMD and the abundance pattern. Although this solution is not unique, the use of a large number of spectral lines with a good temperature coverage constrains the interval of possible solutions to a small range of values around the solution proposed. Error bars for the EMD can be calculated with a Monte Carlo method, consisting of the variation of the observed fluxes by $\pm 1\sigma$ and the determination of the best solution among 1000 possible variations around the initial EMD solution. Such an exercise is performed for 1000 sets of possible line fluxes, providing error bars for the solution. The abundances of the different elements are determined during the calculation of the EMD, with error bars resulting from the quadratic summation of the errors on the measurement of observed fluxes ($\Delta F_{\rm obs}/F_{\rm obs}$), and the dispersion of the predicted-to-observed line ratios $[(F_{\rm obs} - F_{\rm pred})/F_{\rm obs}]$ of lines of the same element (the latter permits us to evaluate indirectly the errors related to atomic models). The abundances of the elements are determined *relative* to Fe, with the [Fe/H] abundance derived afterwards from the best fit to the global spectrum for the given EMD and abundances pattern. The coronal abundances determined, with their photospheric counterparts are shown in Figs. 2 and 3, and are listed in Table 2. EMD distributions (Table 3) are shown in Fig. 4. The line fluxes measured in the four targets are listed in Tables 4–7[1].

4. Results

4.1. Procyon

Procyon (α CMi A, HR 2943, HD 61421) is a well-studied nearby F4IV star (3.497 pc Perryman et al., 1997). A rotational period of $\sim$ 9.1 d can be deduced from $v \sin i$ = 6.1

[1] These tables are available in electronic format only.

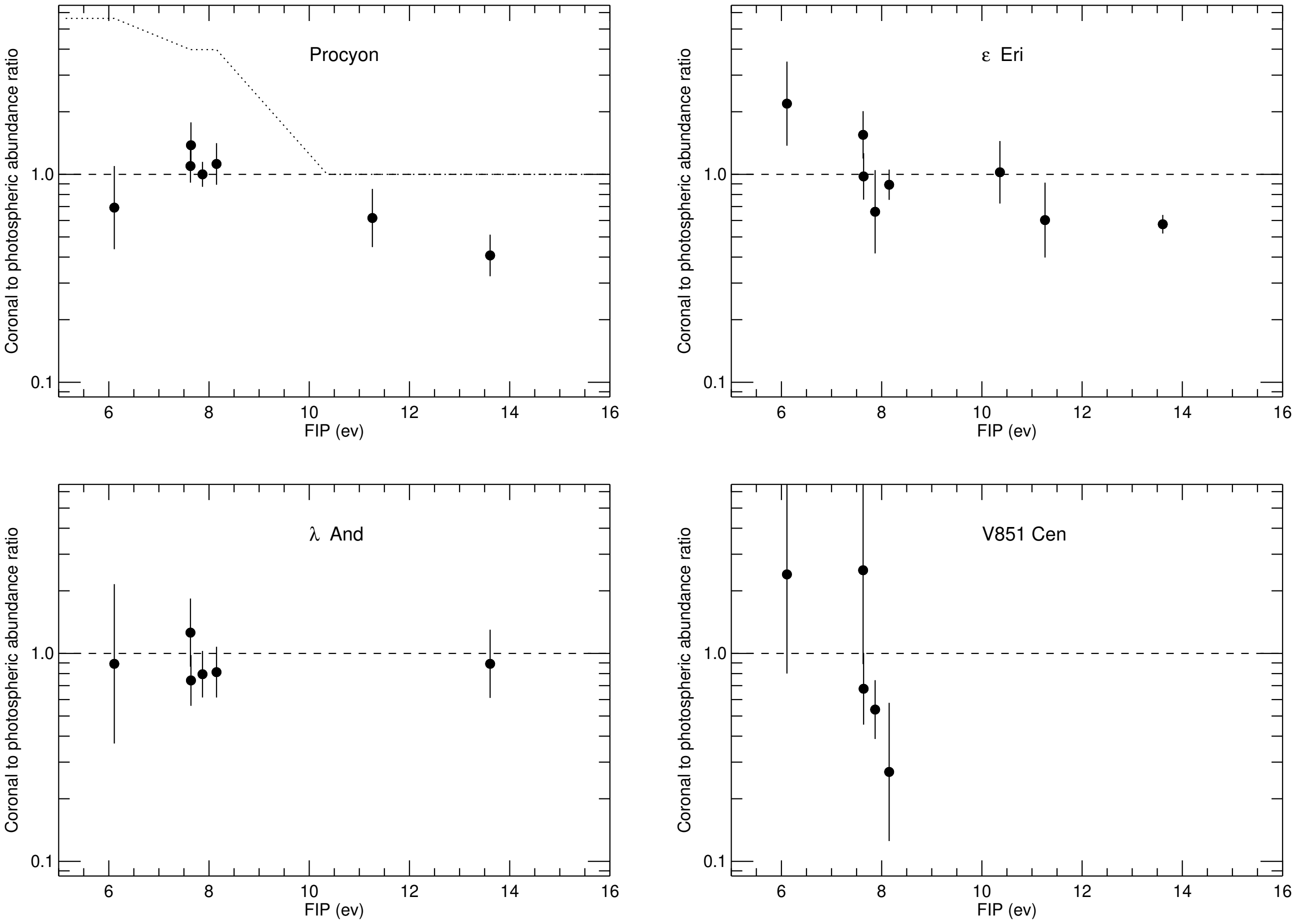

Fig. 3. Coronal to photospheric abundance ratio for Procyon, ϵ Eri, λ And and V851 Cen, with 1σ error bars. Solar coronal (at $\log T[K] \sim 6.1$) to photospheric abundance ratios (Feldman & Laming, 2000) are indicated with a dotted line in the Procyon plot.

km/s (de Medeiros & Mayor, 1999) and $i = 32°$(Irwin et al., 1992). Photospheric abundances of different elements have been determined by many authors, resulting in a metallicity close to solar. In this work we will use the values calculated by Edvardsson et al. (1993), with C abundance from Varenne & Monier (1999). First studies on the coronal abundances were carried out using EUVE observations: Drake et al. (1995) calculated, using a line-based analysis, the EMD for low and high FIP elements separately, but they did not find any "FIP" or "inverse FIP" effect. Global fits to *Chandra*/LETG and XMM-*Newton* high-resolution spectra were employed by Raassen et al. (2002) to determine the abundances of Procyon, also concluding that no FIP-related effects are present in the corona of Procyon (although no comparison with photospheric values is present in their study).

In the present work line fluxes were corrected from the ISM assuming a value of $\log N_{\rm H}({\rm cm}^{-2}) \sim 18.2$ (Sanz-Forcada et al., 2003a). Several problems affect the analysis of the *Chandra* Procyon spectra. First, the shape of the continuum of a relatively cool corona like that of Procyon, in the wavelength range covered here, does not allow us to establish the [Fe/H] coronal abundance accurately (a wide range of values show similar line-to-continuum ratios), thus we fixed it at its photospheric value (note that the rest of coronal abundances are calculated relative to Fe, and the general level of the EMD depends on [Fe/H] too). Also, the determination of coronal abundances is affected, in the LETG wavelength range, by the lack of a complete temperature coverage provided by Fe (only two lines are formed at $\log\ T[K] \lesssim 6.2$), while many lines from other elements have little temperature overlap with Fe lines. However it is possible to include in the analysis the Fe lines observed with EUVE (Fe XI–XVI), obtaining a better temperature coverage for one element, useful for the determination of abundances of other elements. Measurements of EUVE Fe line fluxes in the range 170–370 Å were made by Sanz-Forcada et al. (2003a) from observations taken in 1993, 1994 and 1999 (the latter is partially simultaneous with the LETG campaign, and no substantial changes were detected in the EUV flux level). The inclusion of the EUVE lines allows us to cover the range $\log\ T(K) \sim 5.6$–6.8, where almost all lines of other elements are also formed.

The abundances determined for Procyon do not show substantial differences between photospheric and coronal relative abundances (note that no error bars are published for the photospheric abundances), with the most notable difference being a relative underabundance of O in the corona. Nevertheless,

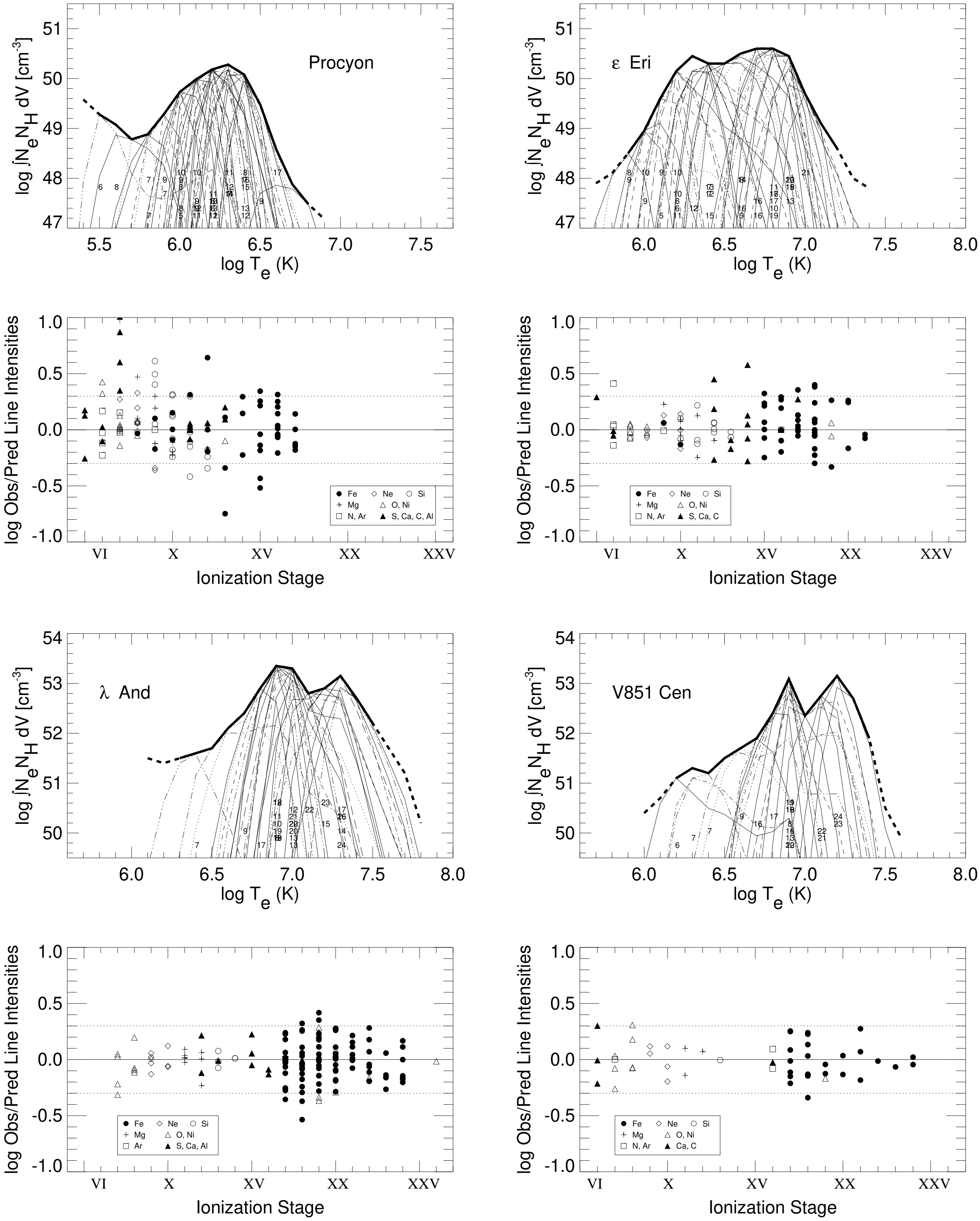

Fig. 4. Emission Measure Distribution for Procyon, ϵ Eri, λ And and V851 Cen. Thin lines represent the relative contribution function for each ion (the emissivity function multiplied by the EMD at each point). Small numbers indicate the ionization stages of the species. Also plotted are the observed to predicted line flux ratios for the ion stages in the upper figure. The dotted lines denote a factor of 2.

Table 2. Coronal and photospheric abundances of the elements ([X/H], solar units) in the target stars.

X	FIP	Reference[a]	Procyon		ϵ Eri		λ And		V851 Cen	
	eV	solar value	Photosphere	Corona[b]	Photosphere	Corona	Photosphere	Corona	Photosphere	Corona
Al	5.98	6.47	0.00	0.45± 0.12	−0.12± 0.02	…	…	−0.05± 0.17	0.25± 0.05	…
Ca	6.11	6.36	−0.04	−0.20± 0.20	−0.11± 0.03	0.23± 0.20	−0.20± 0.10	−0.25± 0.37	0.12± 0.08	0.50± 0.47
Ni	7.63	6.25	0.02	0.06± 0.08	−0.20± 0.03	−0.01± 0.11	−0.40± 0.10	−0.30± 0.13	−0.30± 0.10	0.10± 0.44
Mg	7.64	7.58	0.07	0.21± 0.11	−0.14± 0.05	−0.15± 0.10	−0.10± 0.10	−0.23± 0.07	0.05± 0.03	−0.12± 0.17
Fe	7.87	7.67	−0.18	−0.18± 0.06	−0.12± 0.01	−0.30± 0.20	−0.50± 0.10	−0.60± 0.05	−0.23± 0.10	−0.50± 0.10
Si	8.15	7.55	0.01	0.06± 0.10	−0.16± 0.02	−0.21± 0.07	−0.30± 0.10	−0.39± 0.07	−0.05± 0.09	−0.62± 0.32
S	10.36	7.21	…	−0.23± 0.17	−0.01± 0.01	0.00± 0.15	…	−0.67± 0.16	…	−1.05± 1.33
C	11.26	8.56	0.11	−0.10± 0.14	−0.06	−0.28± 0.18	…	…	…	−0.37± 0.40
O	13.61	8.93	−0.05	−0.44± 0.10	−0.16± 0.02	−0.40± 0.04	−0.25± 0.10	−0.30± 0.13	…	−0.09± 0.23
N	14.53	8.05	…	−0.25± 0.13	…	−0.31± 0.14	…	…	…	0.00± 0.14
Ar	15.76	6.56	…	−0.43± 0.13	…	0.13± 0.14	…	−0.28± 0.26	…	−0.04± 0.54
Ne	21.56	8.09	…	0.02± 0.11	…	0.00± 0.08	…	−0.08± 0.06	…	0.41± 0.13

[a] Solar photospheric abundances from Anders & Grevesse (1989), adopted in this work, are expressed in logarithmic scale. Note that several values have been updated in the literature, most notably the cases of O (now ~8.7, Allende Prieto et al., 2001; Holweger, 2001) and C (now 8.39, Allende Prieto et al., 2002).
[b] The [Fe/H] coronal abundance of Procyon is set to its photospheric value, with nominal error bars determined from the observed-to-predicted fluxes dispersion.

an interesting feature arises when fitting the EMD and abundances. Assuming that the EMD (see Fig. 4) is correct for all elements, higher (relative to Fe) abundance of S, O, Ne, Si and Mg at lower temperatures would improve the fit of their respective lines (the case of the S VII lines is very remarkable), while elements like Ni, Ca, Al, C or N cover a gradient of temperatures too small to reveal any trend. This effect could be also caused by the Fe abundance increasing with temperature, from the minimum of the EMD at $\log T(K) \sim 5.8$ to the maximum at $\log T(K) \sim 6.3$. This might indicate a trend of a mild FIP effect which increases with temperature in the corona of Procyon (Drake et al. 1995 also discuss a possible temperature dependence of the coronal abundances in Procyon). In the solar corona, the FIP effect is indeed larger at $\log T(K) \sim 6.15$ than at $\log T(K) \lesssim 5.9$ (Feldman & Laming, 2000). Although suggestive, this hypothesis cannot presently be confirmed with high confidence for Procyon given the present uncertainties in atomic models and in the determination of the EMD of this star. Similarly, an increase in the [Ne/Fe] abundance with temperature between $\log T(K) \sim 5.8$ and $\log T(K) \sim 6.6$ would explain the discrepancies found in the determination of the coronal Ne abundance of AD Leo from Ne VIII lines (Sanz-Forcada & Micela, 2002) and from Ne IX and Ne X lines (Maggio et al., 2002).

4.2. ϵ Eri

As one of the nearest cool stars ($d = 3.22$ pc), ϵ Eri (HD 22049, HR 1084) is frequently studied for its activity, abundances, and more recently, stellar planetary companions (see e.g., Hatzes et al., 2000). With $P_{\rm phot} \sim 11.3$ d (Baliunas et al., 1983), ϵ Eri (K2V) has an intermediate activity level. Photospheric abundances derived by Zhao et al. (2002) are used here for comparison with the coronal values, and a value of $\log N_{\rm H}({\rm cm}^{-2}) \sim 18.1$ (Sanz-Forcada et al., 2003a) is adopted to correct for ISM absorption. The first high-resolution analysis on coronal abundances of ϵ Eri was made by Laming et al. (1996) who analyzed EUVE spectra, calculating separate line-based EMDs for low- and high-FIP elements, concluding that a solar-like FIP effect was present in the corona of ϵ Eri. Coronal electron density diagnostics were reported by Ness et al. (2002) from the *Chandra*/LETG observations of ϵ Eri.

In the present work we derive the coronal abundance of 11 elements from the *Chandra*/LETG spectrum of ϵ Eri. The corona is dominated by emitting material in the range $\log T(K) \sim 5.8$–7.2, with a distribution compatible with the presence of a peak at $\log T(K) \sim 6.5$ as EUVE data suggest (Sanz-Forcada et al., 2003a), but also with two peaks at $\log T(K) \sim 6.3$ and 6.8, as the present data, also compatible with EUVE fluxes, suggest. The [Fe/H] coronal abundance is better constrained than for Procyon, with a 0.2 dex uncertainty; the agreement between predicted and observed fluxes is also better than for Procyon. A mild FIP-like bias is detected in the corona of ϵ Eri, affecting only Ca and Ni (Fig. 3), with a progressive lower coronal abundance for elements with higher FIP – while in the Sun the FIP effect consists of a enhancement by more than a factor of 3 of the elements with FIP $\lesssim 10$ eV.

4.3. λ And

λ And (HD 222107, HR 8961) is an active binary system with a G8 IV-III primary and an unseen companion in an orbit with $P_{\rm orb} = 20.5212$ d (Walker, 1944). λ And is one of the few active stars for which measurements of photospheric abundances for a good number of elements (Savanov & Berdyugina, 1994; Donati et al., 1995) are available, also thanks to its low rotation rate ($P_{\rm phot} = 54.33$ d, Perryman et al., 1997). Coronal abundances from high resolution spectra were not obtained from EUVE data because the ISM absorption did not allow the measurement of fluxes of lines for elements other than Fe (although the spectrum is suggestive of a low value of [Fe/H], see Sanz-Forcada et al., 2001), and the global fit of the XMM/RGS spec-

Table 3. Emission Measure Distribution of the target stars

$\log T$ (K)	$\log \int N_e N_H dV$ (cm^{-3})[a] Procyon	ϵ Eri	λ And	V851 Cen
5.4	49.58	…	…	…
5.5	$49.28^{+0.55}_{-0.05}$	…	…	…
5.6	$49.08^{+0.40}_{-0.30}$	…	…	…
5.7	$48.78^{+0.20}_{-0.40}$	47.60	…	…
5.8	$48.88^{+0.20}_{-0.40}$	47.80	…	…
5.9	$49.28^{+0.20}_{-0.20}$	$48.20^{+0.20}_{-0.30}$	…	…
6.0	$49.73^{+0.05}_{-0.40}$	$48.65^{+0.20}_{-0.30}$	…	50.40
6.1	$49.98^{+0.40}_{-0.05}$	$49.30^{+0.20}_{-0.20}$	50.90	50.70
6.2	$50.18^{+0.05}_{-0.20}$	$49.85^{+0.10}_{-0.20}$	50.80	$51.10^{+0.05}_{-0.40}$
6.3	$50.28^{+0.05}_{-0.10}$	$50.15^{+0.10}_{-0.20}$	$50.90^{+0.20}_{-0.30}$	$51.30^{+0.05}_{-0.35}$
6.4	$50.08^{+0.10}_{-0.05}$	$50.00^{+0.20}_{-0.10}$	$51.00^{+0.20}_{-0.30}$	$51.20^{+0.05}_{-0.35}$
6.5	$49.48^{+0.05}_{-0.30}$	$50.00^{+0.20}_{-0.30}$	$51.10^{+0.20}_{-0.30}$	$51.50^{+0.10}_{-0.40}$
6.6	$48.58^{+0.20}_{-0.40}$	$50.20^{+0.20}_{-0.20}$	$51.50^{+0.10}_{-0.40}$	$51.70^{+0.20}_{-0.40}$
6.7	$47.88^{+0.30}_{-0.40}$	$50.30^{+0.15}_{-0.25}$	$51.80^{+0.05}_{-0.35}$	$51.90^{+0.05}_{-0.35}$
6.8	$47.48^{+0.30}_{-0.40}$	$50.30^{+0.05}_{-0.35}$	$52.30^{+0.05}_{-0.15}$	$52.40^{+0.05}_{-0.30}$
6.9	47.18	$50.15^{+0.15}_{-0.05}$	$52.75^{+0.05}_{-0.05}$	$53.09^{+0.05}_{-0.05}$
7.0	…	$49.40^{+0.40}_{-0.10}$	$52.70^{+0.15}_{-0.05}$	$52.35^{+0.20}_{-0.30}$
7.1	…	$48.80^{+0.40}_{-0.30}$	$52.20^{+0.05}_{-0.20}$	$52.75^{+0.20}_{-0.20}$
7.2	…	$48.30^{+0.30}_{-0.30}$	$52.30^{+0.05}_{-0.40}$	$53.15^{+0.05}_{-0.30}$
7.3	…	47.70	$52.55^{+0.05}_{-0.40}$	$52.70^{+0.30}_{-0.20}$
7.4	…	47.50	$52.10^{+0.20}_{-0.30}$	$51.90^{+0.40}_{-0.40}$
7.5	…	…	$51.60^{+0.40}_{-0.30}$	50.50
7.6	…	…	51.10	50.50
7.7	…	…	50.60	…
7.8	…	…	49.60	…

[a] Emission Measure, where N_e and N_H are electron and hydrogen densities, in cm^{-3}. Error bars provided are not independent between the different temperatures, see text.

tra gave no clear trend with FIP (Audard et al., 2003). A preliminary analysis of the *Chandra*/HETG and LETG spectra was reported by Dupree et al. (2000) and Brickhouse et al. (2003) respectively.

The low ISM absorption[2] ($\log N_H[\mathrm{cm}^{-2}] = 18.45$, Wood et al., 1996) makes the correction of fluxes unnecessary (affecting the line fluxes at less than the 1% level). The high spectral resolution and good statistics achieved in the observation allow us to obtain the best determination of the element abundances of the four stars, also supported by a good agreement between observed and predicted fluxes for most lines. The fluxes measured in the EUV range (Sanz-Forcada et al., 2001) are also well predicted using the EMD determined here. The coronal abundances determined here are remarkably consistent with the photospheric values calculated by Donati et al. (1995), and they are also close to the values calculated by Savanov & Berdyugina (1994).

[2] Note that this value of the ISM absorption, combined with the distance to the star, is too high to see lines from elements other than Fe that were measured for other stars (usually at $\lambda \gtrsim 200$ Å) with EUVE, but it is a low value to notice its effects in the HETG spectral range.

4.4. V851 Cen

V851 Cen (HD 119285) is an active binary system with a K2IV-III primary and an unseen companion, with a photometric period of 12.05 d (Lloyd Evans & Koen, 1987; Cutispoto et al., 2001), slightly longer than its orbital period (P_{orb} = 11.989 d, Saar et al., 1990). V851 Cen has a small projected rotational velocity ($v \sin i$ = 6.5 km s^{-1}, Saar et al., 1990) which allowed Katz et al. (2003) and Morel et al. (2003) to derive accurate photospheric abundances, revising the value of [Fe/H]~ -0.6 determined by Randich et al. (1993) to a value of [Fe/H]~ -0.2. In the present work the coronal abundances and thermal structure of this star is determined for the first time. A correction of the observed fluxes due to the absorption of the ISM was applied, assuming $\log N_H(\mathrm{cm}^{-2}) \sim 19.5$, the value determined for the nearby star β Cen (Fruscione et al., 1994)[3]. We use the photospheric abundances provided by the "Method 1" of Morel et al. (2003), as shown in Fig. 2. When the coronal abundances are compared to solar photospheric ones, V851 Cen shows a behavior very similar to that of stars like AR Lac or AB Dor, with a decrease of abundance with FIP until Si, and a progressive increment for elements with high FIP. However, when these abundances are compared with the stellar photospheric values, the conclusions are different, with only a small depletion of coronal Fe, Mg and Si, and a possible enhancement of the elements with lowest FIP (Ca and Ni), although still consistent with the photospheric values (Fig. 3). The determination of the photospheric abundance of elements with larger FIP would be desirable to confirm any trend.

5. Discussion and conclusions

The results found in the present sample show that the issue of coronal abundances in stars other than the Sun is complex and still poorly understood. Solar coronal abundance is by itself a complex issue, with the actual values depending on which part of the corona is observed (with coronal holes, active regions and flares showing quite different abundance patterns). Results obtained from full disk spectra (thus comparable to stellar spectra) show enhancements by at least a factor of 3 in elements with FIP $\lesssim$ 10 eV (Laming et al., 1995). Young solar active regions show coronal abundance compatible with the photospheric values, but they soon develop a FIP bias that reaches average coronal values in two to three days (Sheeley, 1996; Widing & Feldman, 2001). The FIP effect that is observed in the solar corona seems to disappear with increasing activity level of the star, as it has been shown in cases like II Peg (Huenemoerder et al., 2001), AR Lac (Huenemoerder et al., 2003), AB Dor (Sanz-Forcada et al., 2003b), λ And and V851 Cen. A solar-like FIP effect appears to be present in α Cen A (Raassen et al., 2003), a star very similar to the Sun in many physical parameters, as well as in other solar analogs with low levels of activity, such as π^1 UMa and χ^1 Ori (Güdel et al., 2002), although only the Fe photospheric abundance is

[3] Uncertainties in the determination of the ISM absorption are of minor importance given the small correction (at the $\sim$ 2% level at 20 Å) to be applied to the line fluxes.

known for these two objects (so that abundance patterns assume a solar-like mix). A mid-activity level star, ϵ Eri, could be showing the progressive disappearance of the FIP effect, with elements like Mg and Fe already showing photospheric abundances in the corona, and leaving a marginal coronal abundance enhancement only for Ca and Ni. Finally, Procyon seems to be quite different to the Sun, with no FIP-related trends evident, although there could be an increment of Fe abundance with the coronal temperature relative to other elements with higher FIP (see Sect. 4.1). The FIP effect detected in the solar corona above quiet regions grows with temperature, in a range similar to that covered here for Procyon (Feldman & Laming, 2000).

The interpretation of the metal depletion in the corona of active stars that has been given in the past from initial results is somewhat in contradiction with the present results. Many of the stars for which a "metal abundance deficiency syndrome" (MAD) has been claimed do not have measurements of the photospheric abundance available (or they are limited to Fe abundance determinations), and published work is limited to the comparison of stellar coronal patterns with solar photospheric abundances (a rather arbitrary practice). The case of λ And is quite remarkable, with compatible coronal and photospheric abundances for all elements tested, and a definitely non-solar photospheric abundance pattern. V851 Cen, with a similar coronal thermal structure (Fig. 4) shows a marginal coronal abundance depletion. Other cases like II Peg (Huenemoerder et al., 2001) or AR Lac (Huenemoerder et al., 2003) also show moderate depletion when they are compared to the respective photospheric values, but strong metal depletion seems to be clear only for AB Dor (Sanz-Forcada et al., 2003b, and references therein). However AB Dor is a fast rotator, and the only available determination of photospheric abundances, carried out by Vilhu et al. (1987), needs further confirmation given the difficulty of the measurements in a spectrum so highly affected by rotational broadening.

While the absence of a FIP effect in active stars, at least at the solar level, is well supported at this point, the presence of a general "MAD effect" or an "inverse FIP effect" increasing with activity is not yet clearly established, given the discrepancies found between stars with quite similar levels of activity and thermal coronal structure like AB Dor, λ And and V851 Cen. Moreover, the abundance pattern could also be changing in different parts of the corona, depending on the coronal temperature, as present in Procyon. A larger sample of stars with both photospheric and coronal abundances, determined in a homogeneous way, would be necessary to establish a general trend between coronal abundances and activity levels.

Acknowledgements. We acknowledge support by the Marie Curie Fellowships Contract No. HPMD-CT-2000-00013. We have made use of data obtained through the *Chandra* data archive, operated by the Smithsonian Astrophysical Observatory for NASA. This research has also made use of NASA's Astrophysics Data System Abstract Service. We are grateful to the referee, Dr. J. M. Laming, for the careful reading and useful comments brought to the manuscript.

References

Allende Prieto, C., Lambert, D. L., & Asplund, M. 2001, ApJ, 556, L63
Allende Prieto, C., Lambert, D. L., & Asplund, M. 2002, ApJ, 573, L137
Anders, E. & Grevesse, N. 1989, Geochim. Cosmochim. Acta, 53, 197
Audard, M., Güdel, M., Sres, A., Raassen, A. J. J., & Mewe, R. 2003, A&A, 398, 1137
Baliunas, S. L., Hartmann, L., Noyes, R. W., et al. 1983, ApJ, 275, 752
Brickhouse, N. S., Dupree, A. K., & Hoogerwerf, R. 2003, AAS/High Energy Astrophysics Division, 35
Brinkman, A. C., Behar, E., Güdel, M., et al. 2001, A&A, 365, L324
Cayrel de Strobel, G., Soubiran, C., & Ralite, N. 2001, A&A, 373, 159
Cutispoto, G., Messina, S., & Rodonò, M. 2001, A&A, 367, 910
de Medeiros, J. R. & Mayor, M. 1999, A&AS, 139, 433
den Herder, J. W., Brinkman, A. C., Kahn, S. M., et al. 2001, A&A, 365, L7
Donati, J.-F., Henry, G. W., & Hall, D. S. 1995, A&A, 293, 107
Drake, J. J. 2002, in ASP Conf. Ser. 277: Stellar Coronae in the Chandra and XMM-Newton Era, 75
Drake, J. J., Brickhouse, N. S., Kashyap, V., et al. 2001, ApJ, 548, L81
Drake, J. J., Laming, J. M., & Widing, K. G. 1995, ApJ, 443, 393
Drake, J. J., Laming, J. M., & Widing, K. G. 1997, ApJ, 478, 403
Drake, S. A. 1996, in ASP Conf. Ser. 99: Cosmic Abundances, ed. by S. S. Holt & G. Sonneborn, 215
Dupree, A. K., Brickhouse, N. S., & Drake, J. J. 2000, Bulletin of the American Astronomical Society, 32, 1256
Edvardsson, B., Andersen, J., Gustafsson, B., et al. 1993, A&A, 275, 101
Favata, F. & Micela, G. 2003, Space Sci. Rev., in press
Feldman, U. & Laming, J. M. 2000, Phys. Scr, 61, 222
Fruscione, A., Hawkins, I., Jelinsky, P., & Wiercigroch, A. 1994, ApJS, 94, 127
Güdel, M., Audard, M., Sres, A., et al. 2002, in ASP Conf. Ser. 277: Stellar Coronae in the Chandra and XMM-Newton Era, 497
Hatzes, A. P., Cochran, W. D., McArthur, B., et al. 2000, ApJ, 544, L145
Holweger, H. 2001, in Joint SOHO/ACE workshop "Solar and Galactic Composition", ed. R. F. Wimmer-Schweingruber (New York: Springer), AIP Conf. Proc. 598, 23
Houck, J. C. & Denicola, L. A. 2000, in ASP Conf. Ser. 216: Astronomical Data Analysis Software and Systems IX, ed. by N. Manset, C. Veillet, and D. Crabtree (San Francisco: ASP), 591
Huenemoerder, D. P., Canizares, C. R., Drake, J. J., & Sanz-Forcada, J. 2003, ApJ, 595, 1131
Huenemoerder, D. P., Canizares, C. R., & Schulz, N. S. 2001, ApJ, 559, 1135
Irwin, A. W., Fletcher, J. M., Yang, S. L. S., Walker, G. A. H., & Goodenough, C. 1992, PASP, 104, 489

Katz, D., Favata, F., Aigrain, S., & Micela, G. 2003, A&A, 397, 747
Kelly, R. L. 1987, Atomic and ionic spectrum lines below 2000 Angstroms. Hydrogen through Krypton (New York: American Institute of Physics, Amer. Chem. Soc. and the Nat. Bureau of Standards, 1987)
Laming, J. M. & Drake, J. J. 1999, ApJ, 516, 324
Laming, J. M., Drake, J. J., & Widing, K. G. 1995, ApJ, 443, 416
Laming, J. M., Drake, J. J., & Widing, K. G. 1996, ApJ, 462, 948
Lloyd Evans, T. & Koen, M. C. J. 1987, South African Astronomical Observatory Circular, 11, 21
Maggio, A., Drake, J. J., Kashyap, V., et al. 2002, in ASP Conf. Ser. 277: Stellar Coronae in the Chandra and XMM-Newton Era, 57
Morel, T., Micela, G., Favata, F., Katz, D., & Pillitteri, I. 2003, A&A, submitted
Ness, J.-U., Schmitt, J. H. M. M., Burwitz, V., et al. 2002, A&A, 394, 911
Perryman, M. A. C., Lindegren, L., Kovalevsky, J., et al. 1997, A&A, 323, L49
Raassen, A. J. J., Mewe, R., Audard, M., et al. 2002, A&A, 389, 228
Raassen, A. J. J., Ness, J.-U., Mewe, R., et al. 2003, A&A, 400, 671
Randich, S., Gratton, R., & Pallavicini, R. 1993, A&A, 273, 194
Saar, S. H., Nordstrom, B., & Andersen, J. 1990, A&A, 235, 291
Sanz-Forcada, J., Brickhouse, N. S., & Dupree, A. K. 2001, ApJ, 554, 1079
Sanz-Forcada, J., Brickhouse, N. S., & Dupree, A. K. 2003a, ApJS, 145, 147
Sanz-Forcada, J., Maggio, A., & Micela, G. 2003b, A&A, 408, 1087
Sanz-Forcada, J. & Micela, G. 2002, A&A, 394, 653
Savanov, I. S. & Berdyugina, S. V. 1994, Astronomy Letters, 20, 227
Sheeley, N. R. 1996, ApJ, 469, 423
Smith, R. K., Brickhouse, N. S., Liedahl, D. A., & Raymond, J. C. 2001, ApJ, 556, L91
Varenne, O. & Monier, R. 1999, A&A, 351, 247
Vilhu, O., Gustafsson, B., & Edvardsson, B. 1987, ApJ, 320, 850
Walker, E. C. 1944, JRASC, 38, 249
Weisskopf, M. C., Brinkman, B., Canizares, C., et al. 2002, PASP, 114, 1
White, N. E., Arnaud, K., Day, C. S. R., et al. 1994, PASJ, 46, L97
Widing, K. G. & Feldman, U. 2001, ApJ, 555, 426
Wood, B. E., Alexander, W. R., & Linsky, J. L. 1996, ApJ, 470, 1157
Zhao, G., Chen, Y. Q., Qiu, H. M., & Li, Z. W. 2002, AJ, 124, 2224

Online Material

Table 4. Chandra/LETG line fluxes of Procyon[a]

Ion	$\lambda_{\rm model}$	log $T_{\rm max}$	$F_{\rm obs}$	S/N	ratio	Blends
Fe xvii	12.1240	6.8	6.03e-15	3.6	-0.18	Ne x 12.1321, Ne x 12.1375
Ne ix	13.4473	6.6	2.79e-14	8.3	-0.34	
Ne ix	13.6990	6.6	1.53e-14	6.2	-0.36	Ne ix 13.7130
Fe xvii	15.0140	6.7	2.71e-14	8.8	-0.15	
Fe xvii	15.2610	6.7	2.45e-14	8.5	0.00	O viii 15.1760, 15.1765, Fe xvii 15.2509, 15.2615, 15.2797
O viii	16.0055	6.5	3.04e-14	8.3	0.07	O viii 16.0067
Fe xvii	16.7800	6.7	1.44e-14	6.8	-0.12	
Fe xvii	17.0510	6.7	5.22e-14	12.0	0.14	Fe xvii 17.0960
O vii	17.3960	6.4	5.25e-15	3.8	-0.01	
O vii	17.7680	6.4	1.69e-14	6.9	0.13	
O vii	18.6270	6.3	4.76e-14	12.3	0.04	
O viii	18.9671	6.5	1.88e-13	24.7	-0.05	O viii 18.9725
N vii	20.9095	6.3	1.26e-14	5.4	0.15	N vii 20.9106
O vii	21.6015	6.3	2.66e-13	25.1	-0.14	
O vii	21.8036	6.3	7.20e-14	13.0	0.02	
O vii	22.0977	6.3	2.42e-13	24.0	0.03	
N vii	24.7792	6.3	7.00e-14	13.6	-0.02	N vii 24.7846
N vi	24.8980	6.2	5.64e-15	3.9	-0.12	
C vi	28.4652	6.2	2.85e-14	9.0	0.02	
N vi	28.7870	6.2	5.09e-14	11.9	-0.03	
N vi	29.0843	6.1	1.97e-14	7.4	0.17	
N vi	29.5347	6.1	1.69e-14	6.7	-0.23	
Ca xi	30.4710	6.3	2.19e-14	5.1	0.01	S xiv 30.4270
No id.	31.0340	…	1.69e-14	5.0	…	Si xii 31.015
C vi	33.7342	6.1	2.44e-13	25.8	-0.10	C vi 33.7396
C v	34.9728	6.0	1.85e-14	7.2	0.17	
S xiii	35.6670	6.4	2.66e-14	8.6	0.09	Ca xi 35.6340, 35.7370
S xii	36.3980	6.4	1.55e-14	6.5	0.06	
S xii	36.5730	6.4	1.01e-14	5.2	-0.17	S xii 36.5640
S xiii	37.5980	6.4	1.24e-14	5.5	0.20	S xii 37.5670
S xi	39.2400	6.3	4.48e-14	10.2	0.06	S xi 39.3000, 39.3200
C v	40.2674	6.0	1.06e-13	12.2	0.13	
No id.	40.7250	…	9.27e-14	9.2	…	C v 40.731
C v	41.4715	6.0	3.68e-14	5.7	-0.26	Ar ix 41.4760
No id.	42.5330	…	5.48e-14	7.7	…	S x 42.543
Si xi	43.7630	6.2	3.69e-14	10.8	-0.02	
Si xii	44.0190	6.3	1.38e-14	6.8	-0.24	
Si xii	44.1650	6.3	4.44e-14	12.2	-0.18	Mg x 44.0500, Si xi 44.0690, Si xii 44.1780
No id.	44.4110	…	6.59e-15	4.7	…	
Si xii	45.6910	6.3	1.09e-14	9.1	-0.34	
Si xi	46.2980	6.2	1.47e-14	10.5	0.30	
Si xi	46.3990	6.2	1.61e-14	11.0	-0.15	Si xi 46.4090
Fe xvi	46.7180	6.5	9.39e-15	8.4	0.25	Fe xvi 46.6610
S xi	47.0300	6.3	8.36e-15	5.9	-0.08	Si xi 46.9960, 47.0770, Si x 47.0450
No id.	47.2500	…	1.66e-14	8.3	…	S ix 47.249
No id.	47.4000	…	1.23e-14	7.1	…	S ix 47.433
Si x	47.4890	6.2	1.29e-14	7.3	0.31	
No id.	47.6240	…	1.77e-14	8.5	…	S x 47.655
No id.	47.7500	…	1.12e-14	6.8	…	S x 47.791
No id.	47.8790	…	1.47e-14	7.8	…	Si xi 47.899
Ar ix	48.7390	6.1	7.53e-15	7.5	0.00	Si x 48.6760, 48.7890
Si xi	49.2220	6.2	6.12e-14	21.7	-0.11	
No id.	49.3340	…	1.48e-14	10.7	…	S ix 49.328
Si x	49.7010	6.2	7.39e-15	7.6	0.14	Si x 49.7510
Fe xvi	50.3500	6.5	1.65e-14	11.4	0.20	Si x 50.3160, 50.3330, 50.3590
Si x	50.5240	6.2	6.60e-14	22.8	0.12	Fe xvi 50.5550
Si x	50.7030	6.2	4.43e-14	18.7	-0.24	Si x 50.6910
Si xi	52.2980	6.2	2.53e-14	13.8	-0.42	Si xi 52.2690, Al xi 52.2990
Al xi	52.4460	6.2	9.05e-15	8.3	-0.00	
Si x	52.6110	6.2	9.34e-15	8.5	-0.08	Si x 52.6120
No id.	52.7600	…	1.55e-14	10.8	…	S viii 52.756
Fe xv	52.9110	6.4	9.92e-15	8.8	-0.04	
No id.	53.0480	…	7.36e-15	7.5	…	
Fe xv	53.1100	6.4	6.60e-15	7.0	0.22	Si x 53.1530
Si x	54.5990	6.2	1.10e-14	8.9	0.32	
Si ix	55.1160	6.1	3.04e-14	14.7	0.40	Si ix 55.0390, 55.0940, Ni xvii 55.0390
Si ix	55.3050	6.1	8.40e-14	24.2	0.05	Si ix 55.2340, 55.3830, 55.4010
No id.	56.9000	…	1.53e-14	7.1	…	Si x 56.08
Fe xv	59.4050	6.3	8.68e-15	5.2	-0.52	
S vii	60.1610	5.8	1.13e-14	5.9	0.35	Si x 60.1180
No id.	61.0500	…	5.52e-14	13.1	…	Si viii 61.019
Si ix	61.6490	6.1	3.90e-14	11.0	0.49	Si ix 61.6000, 61.6970
No id.	61.8500	…	2.78e-14	9.3	…	Si ix 61.852
No id.	61.9300	…	2.81e-14	9.3	…	Si viii 61.914
Si x	62.6950	6.2	2.17e-14	8.2	-0.18	Mg ix 62.6610, 62.7510
Fe xvi	62.8790	6.5	1.92e-14	7.7	0.04	
Si ix	62.9750	6.1	9.72e-15	5.5	0.61	
Mg x	63.1520	6.1	2.08e-14	8.0	-0.19	
Mg x	63.2950	6.1	3.82e-14	10.9	-0.23	Mg x 63.3110
Fe xvi	63.7190	6.5	2.25e-14	8.4	-0.21	
Fe xv	63.9580	6.3	1.94e-14	7.8	0.26	
No id.	64.1230	…	2.52e-14	8.8	…	
Mg x	65.6730	6.1	9.77e-15	7.8	-0.22	
Mg x	65.8450	6.1	2.69e-14	13.3	-0.11	Ne viii 65.8940

Table 4. (cont). Chandra/LETG line fluxes of Procyon[a]

Ion	λ_{model}	log T_{max}	F_{obs}	S/N	ratio	Blends
Fe XVI	66.2630	6.5	9.90e-15	7.9	-0.07	
No id.	66.3130	…	9.61e-15	8.0	…	Ne VIII 66.330
Fe XVI	66.3680	6.5	1.58e-14	10.0	-0.04	
Mg IX	67.1350	6.0	1.37e-14	6.3	0.30	Mg IX 67.1410
Mg IX	67.2390	6.0	2.55e-14	8.6	0.19	Mg IX 67.2460
Ne VIII	67.3820	5.9	1.84e-14	7.3	0.33	Si X 67.3550, Ne VIII 67.3860
Fe XV	69.6490	6.3	5.09e-14	18.0	-0.18	
No id.	69.8730	…	3.50e-14	14.8	…	Si VIII 69.825
Fe XV	70.0540	6.3	2.90e-14	13.5	0.34	Fe XV 69.9450, 69.9870
No id.	71.9110	…	1.99e-14	11.1	…	Mg IX 71.901
S VII	72.0280	5.8	1.82e-14	10.6	0.60	Mg IX 72.0280
Mg IX	72.3120	6.0	3.48e-14	14.7	-0.12	
S VII	72.6630	5.8	1.50e-14	9.7	1.01	
S VII	72.8980	5.8	1.47e-14	9.5	0.87	
Fe XV	73.4730	6.3	1.08e-14	8.2	-0.43	Ne VIII 73.4750
Ne VIII	73.5630	5.9	1.07e-14	8.1	0.19	Ne VIII 73.5650
Mg VIII	74.8580	5.9	2.39e-14	11.9	0.10	
Mg VIII	75.0440	5.9	3.01e-14	13.4	-0.02	Mg VIII 75.0340
No id.	76.0310	…	1.96e-14	10.7	…	Fe X 76.006
Mg IX	77.7370	6.0	2.86e-14	12.8	-0.12	
No id.	77.8340	…	1.16e-14	8.1	…	
No id.	79.4950	…	1.23e-14	8.4	…	Fe XII 79.488
No id.	80.5320	…	1.38e-14	8.7	…	Fe XII 80.510
No id.	82.7000	…	2.92e-14	8.6	…	Fe XII 82.744
No id.	83.5980	…	1.02e-14	7.3	…	Mg VIII 83.587
Mg VII	83.9100	5.9	4.07e-15	4.6	-0.01	
No id.	83.9960	…	1.82e-14	9.7	…	Mg VII 84.025
No id.	86.8220	…	1.94e-14	10.1	…	Mg VIII 86.847
Mg VIII	87.0210	5.9	1.50e-14	8.8	0.47	
Ne VIII	88.0820	5.8	5.06e-14	16.2	0.06	Ne VIII 88.1190
No id.	91.8360	…	1.97e-14	10.2	…	Ni X 91.790
No id.	94.0510	…	3.76e-14	13.9	…	Fe X 94.012
No id.	96.0420	…	3.18e-14	12.5	…	Si VI 96.022
No id.	96.1430	…	3.22e-14	12.5	…	Fe X 96.122
Ne VII	97.4950	5.8	1.37e-14	8.0	0.27	
Ne VIII	98.1150	5.8	2.78e-14	11.4	0.06	
Ne VIII	98.2600	5.8	5.25e-14	15.6	0.08	
No id.	100.6000	…	2.42e-14	10.5	…	Mg VIII 100.597
No id.	102.1000	…	6.31e-15	5.3	…	
Ne VIII	102.9110	5.8	1.41e-14	8.0	0.06	
Ne VIII	103.0850	5.8	2.40e-14	10.4	-0.01	
No id.	103.5740	…	3.38e-14	12.3	…	Fe IX 103.566
No id.	103.9370	…	1.42e-14	8.0	…	
No id.	105.2350	…	2.57e-14	10.8	…	Fe IX 105.208
No id.	111.2550	…	1.93e-14	9.4	…	Ca X 111.198
No id.	113.7970	…	1.52e-14	8.3	…	Fe VIII 113.763
O VI	115.8210	5.5	1.34e-14	7.9	0.32	O VI 115.8300
Ne VII	116.6930	5.8	1.13e-14	7.2	-0.00	
No id.	127.7000	…	1.45e-14	6.5	…	Ne VII 127.663
Fe VIII	130.9410	5.7	1.23e-14	6.0	-0.03	
No id.	131.2800	…	2.32e-14	8.2	…	Fe VIII 131.24
No id.	148.4290	…	1.36e-13	20.3	…	Ni XI 148.402
O VI	150.0890	5.5	7.13e-14	14.7	0.43	O VI 150.1250
Ni XII	152.1540	6.2	7.13e-14	14.7	0.01	
Ni XII	154.1620	6.2	3.60e-14	10.4	0.02	
Ni XIII	157.7290	6.2	3.11e-14	9.5	-0.10	Ni XII 157.8130
No id.	158.4290	…	2.20e-14	8.0	…	Ni X 158.377
No id.	160.0590	…	2.26e-14	7.9	…	Ni X 159.977
Ni XII	160.5550	6.2	1.75e-14	6.9	0.06	
No id.	167.5560	…	4.32e-14	9.7	…	Fe VIII 167.486
No id.	168.2090	…	6.75e-14	11.8	…	Fe VIII 168.172
Fe IX	171.0730	5.9	8.75e-13	29.7	-0.17	

[a] Line fluxes (in erg cm^{-2} s^{-1}) measured in Chandra/LETG Procyon summed spectra. log T_{max} indicates the maximum temperature (K) of formation of the line (unweighted by the EMD). "Ratio" is the log (F_{obs}/F_{pred}) of the line. Blends amounting to more than 5% of the total flux for each line are indicated. For some lines not identified in APED, a tentative identification is suggested in the "Blends" column based on Kelly (1987).

Table 5. Chandra/LETG line fluxes of ϵ Eri[a]

Ion	$\lambda_{\rm model}$	log $T_{\rm max}$	$F_{\rm obs}$	S/N	ratio	Blends
Si xiii	6.6479	7.0	4.57e-14	8.0	-0.07	Si xiii 6.6882
Si xiii	6.7403	7.0	2.35e-14	5.7	-0.02	Si xiii 6.7388, 6.7432
Mg xii	8.4192	7.0	3.00e-14	6.8	-0.10	Mg xii 8.4246
Mg xi	9.1687	6.8	4.95e-14	8.4	-0.25	
Mg xi	9.2312	6.8	7.83e-14	10.5	0.12	Mg xi 9.3143
Ne x	9.7080	6.8	1.65e-14	4.8	-0.00	Ne x 9.7080, 9.7085, Fe xix 9.6938
Ne x	10.2385	6.8	3.31e-14	6.8	-0.17	Ne x 10.2396
Fe xvii	11.2540	6.8	4.85e-14	8.6	-0.01	Fe xviii 11.3260
Fe xviii	11.5270	6.9	4.99e-14	8.9	-0.05	Fe xviii 11.5270, Ne ix 11.5440
Ne x	12.1320	6.8	3.15e-13	22.8	0.14	Ne x 12.1321
Fe xxi	12.2840	7.0	7.90e-14	11.5	-0.08	Fe xvii 12.2660
Ni xix	12.4350	6.9	6.62e-14	10.6	0.06	Fe xxi 12.3930
Fe xx	12.5760	7.0	1.38e-14	4.9	0.26	Fe xx 12.5760, Fe xxi 12.5698
Fe xxi	12.6490	7.0	1.20e-14	4.5	-0.04	Ni xix 12.6560
No id.	12.7550	…	1.30e-14	4.8	…	Fe xxii 12.7540
Fe xx	12.8240	7.0	4.33e-14	8.7	-0.17	Fe xx 12.8460, 12.8640
Fe xx	12.9650	7.0	4.09e-14	8.5	0.24	Fe xx 12.9120, 12.9920, Fe xix 12.9330
Ne ix	13.4473	6.6	4.98e-13	30.6	0.07	Fe xix 13.5180, Ne ix 13.5531
Ne ix	13.6990	6.6	2.01e-13	19.6	0.13	
Fe xvii	13.8250	6.8	1.18e-13	15.1	0.03	Fe xix 13.7458, 13.7950, Ni xix 13.7790, Fe xvii 13.8920
Fe xviii	13.9530	6.9	3.45e-14	8.2	0.40	Fe xix 13.9549, 13.9551, Fe xx 13.9620
Ni xix	14.0430	6.8	4.48e-14	9.4	-0.06	Fe xxi 14.0080, Ni xix 14.0770
Fe xviii	14.2080	6.9	1.09e-13	14.7	-0.17	Fe xviii 14.2080
Fe xviii	14.2560	6.9	4.82e-14	9.8	0.09	Fe xviii 14.2560, Fe xx 14.2670
Fe xviii	14.3430	6.9	9.73e-14	14.0	0.06	Fe xviii 14.3730, 14.4250, 14.4392
Fe xviii	14.5710	6.9	6.44e-14	11.6	0.09	Fe xviii 14.5340, 14.6011
Fe xix	14.6640	6.9	2.65e-14	7.5	0.26	Fe xviii 14.6884
Fe xvii	15.0140	6.7	6.12e-13	36.4	-0.05	
Fe xvii	15.2610	6.7	3.56e-13	28.1	0.13	O viii 15.1760
Fe xvii	15.4530	6.7	6.57e-14	12.0	0.36	Fe xviii 15.4940
Fe xviii	15.6250	6.8	3.52e-14	8.9	-0.05	
Fe xviii	15.7590	6.8	1.35e-14	5.6	0.38	
Fe xviii	15.8240	6.8	3.61e-14	9.1	-0.03	Fe xviii 15.8700
Fe xviii	15.9310	6.8	1.60e-14	6.0	0.24	
O viii	16.0055	6.5	1.75e-13	20.0	0.03	Fe xviii 16.0040, O viii 16.0067
Fe xviii	16.0710	6.8	9.38e-14	14.8	-0.00	Fe xix 16.1100, Fe xviii 16.1590
Fe xvii	16.3500	6.7	1.93e-14	6.9	0.09	Fe xviii 16.3200, Fe xix 16.3414
Fe xvii	16.7800	6.7	3.12e-13	27.5	0.01	
Fe xvii	17.0510	6.7	8.11e-13	41.0	0.13	Fe xvii 17.0960
O vii	18.6270	6.3	4.60e-14	10.5	-0.07	
Ca xviii	18.7320	6.9	6.14e-15	3.8	-0.03	Ca xviii 18.6910, Ar xvi 18.6960
No id.	18.7870	…	9.36e-15	4.8	…	
O viii	18.9671	6.5	7.31e-13	42.4	-0.02	O viii 18.9725
N vii	20.9095	6.3	1.04e-14	4.2	-0.08	N vii 20.9106
Ca xvii	21.1980	6.8	2.31e-14	6.3	0.27	
Ca xvi	21.4500	6.7	9.30e-15	4.1	0.00	
O vii	21.6015	6.3	3.98e-13	26.6	-0.02	
No id.	21.7100	…	2.18e-14	6.2	…	
O vii	21.8036	6.3	8.64e-14	12.4	0.04	
No id.	22.0220	…	1.61e-14	5.4	…	
O vii	22.0977	6.3	2.64e-13	21.8	0.05	
S xiv	24.2850	6.5	1.89e-14	6.1	0.58	S xiv 24.2890
N vii	24.7792	6.3	8.76e-14	13.2	-0.02	N vii 24.7846
N vi	24.8980	6.2	1.14e-14	4.8	0.04	Ar xvi 24.8540
Ar xvi	24.9910	6.7	1.03e-14	4.5	-0.00	
C vi	28.4652	6.2	2.41e-14	7.2	-0.05	C vi 28.4663
N vi	28.7870	6.2	2.24e-14	6.9	-0.14	
N vi	29.0843	6.1	2.14e-14	6.7	0.41	
N vi	29.5347	6.1	1.45e-14	5.4	0.03	
S xiv	30.4270	6.5	3.95e-14	8.3	-0.28	S xiv 30.4690, Ca xi 30.4710
No id.	32.2410	…	2.76e-14	7.6	…	
S xiv	32.4160	6.5	2.14e-14	6.7	0.05	
S xiv	32.5600	6.5	3.20e-14	8.1	-0.08	S xiv 32.5750
S xiv	33.5490	6.5	2.45e-14	7.1	0.13	
C vi	33.7342	6.1	1.76e-13	19.1	-0.01	C vi 33.7396
S xiii	35.6670	6.4	3.66e-14	8.8	-0.17	Ca xi 35.6340, 35.7370
S xii	36.3980	6.4	3.44e-14	8.4	0.19	
S xiii	37.5980	6.4	1.81e-14	5.8	-0.09	
No id.	37.9500	…	3.67e-14	8.2	…	(O viii 18.97, 2nd order)
C v	40.2674	6.0	4.11e-14	6.7	0.29	S xi 40.2730
S xii	43.6510	6.4	9.55e-15	6.7	0.45	
Si xi	43.7630	6.2	2.48e-14	11.7	0.22	
Si xii	44.0190	6.3	3.54e-14	14.0	0.06	Mg x 44.0500, Si xi 44.0690
Si xii	44.1650	6.3	4.95e-14	16.6	0.06	Si xii 44.1780
Si xii	45.5210	6.3	1.05e-14	7.7	0.01	
Si xii	45.6910	6.3	1.98e-14	10.6	-0.02	
Ar ix	48.7390	6.1	6.69e-15	6.2	-0.01	Si x 48.6760, 48.7890
Si xi	49.2220	6.2	3.08e-14	13.4	-0.09	Ar ix 49.1860, Fe xvii 49.2623
Fe xvi	50.3500	6.5	3.51e-14	14.2	0.27	Fe xvii 50.3419
Si x	50.5240	6.2	2.88e-14	12.7	0.10	Fe xvi 50.5550
Si x	50.7030	6.2	1.83e-14	10.0	-0.08	Si x 50.6910

Table 5. (cont). Chandra/LETG line fluxes of ϵ Eri[a]

Ion	$\lambda_{\rm model}$	log $T_{\rm max}$	$F_{\rm obs}$	S/N	ratio	Blends
Si XI	52.2980	6.2	1.98e-14	7.1	-0.12	Si XI 52.2690
Fe XV	52.9110	6.4	2.24e-14	7.6	0.32	
Fe XV	53.1100	6.4	5.83e-15	3.9	0.21	
Fe XVI	54.1420	6.5	2.97e-14	8.8	0.29	
Fe XVI	54.7280	6.5	4.66e-14	11.0	0.19	Fe XVI 54.7630
No id.	56.9000	…	2.61e-14	11.4	…	(O VIII 18.97, 3rd order)
Mg X	57.8760	6.1	3.35e-14	12.8	0.09	Fe XVII 57.9119, Mg X 57.9200
No id.	58.9500	…	1.45e-14	8.3	…	
Fe XV	59.4050	6.3	2.19e-14	10.2	-0.07	
Fe XVI	62.8790	6.5	2.21e-14	7.2	-0.20	
Mg X	63.1520	6.1	1.03e-14	4.9	-0.10	
Mg X	63.2950	6.1	2.59e-14	7.8	0.00	Mg X 63.3110
Fe XVI	63.7190	6.5	5.73e-14	11.6	-0.10	
Fe XV	63.9580	6.3	1.13e-14	5.1	0.07	
Mg X	65.6730	6.1	9.06e-15	6.5	0.07	Ne X 65.6440
Mg X	65.8450	6.1	1.26e-14	7.8	-0.05	Ne VIII 65.8940
Fe XVI	66.2630	6.5	1.93e-14	9.4	-0.10	
No id.	66.3200	…	1.45e-14	8.4	…	(O VII 22.0977, 3rd order)
Fe XVI	66.3680	6.5	3.60e-14	13.0	-0.00	
Fe XV	69.6490	6.3	3.78e-14	13.5	-0.25	
Fe XV	70.0540	6.3	1.94e-14	9.7	0.24	Fe XV 69.9450, 69.9870
No id.	71.9090	…	1.27e-14	5.3	…	Mg IX 71.901
Mg IX	72.3120	6.0	1.10e-14	4.9	0.23	
Fe XV	73.4730	6.3	2.59e-14	11.0	0.00	Ne VIII 73.4750
No id.	76.51700	…	1.47e-14	8.1	…	Fe XVI 76.51
Ne VIII	88.0820	5.8	4.25e-14	12.9	-0.07	Ne VIII 88.0820, 88.1190
Fe XVIII	93.9230	6.8	6.53e-14	16.0	-0.23	
Ne VIII	98.1150	5.8	1.44e-14	7.2	-0.01	
Ne VIII	98.2600	5.8	2.59e-14	9.6	-0.05	Ne VIII 98.2740
Fe XIX	101.5500	6.9	1.03e-14	6.0	-0.33	
Fe XVIII	103.9370	6.8	1.83e-14	8.0	-0.30	
Fe XIX	108.3700	…	1.70e-14	7.7	…	
Fe XXII	117.1700	…	5.72e-15	4.5	…	
Fe XX	121.8300	…	4.77e-15	3.9	…	
Fe XX	132.8500	…	2.94e-14	8.2	…	
Ca XII	141.0380	6.3	1.61e-14	4.8	-0.27	Ca XII 141.0380
Fe IX	171.0730	5.9	1.45e-13	10.8	0.06	
Fe X	174.5340	6.0	7.62e-14	7.3	-0.13	

[a] Line fluxes (in erg cm^{-2} s^{-1}) measured in Chandra/LETG ϵ Eri spectrum. log $T_{\rm max}$ indicates the maximum temperature (K) of formation of the line (unweighted by the EMD). "Ratio" is the log($F_{\rm obs}/F_{\rm pred}$) of the line. Blends amounting to more than 5% of the total flux for each line are indicated. The lines in the range $\lambda\lambda$108–133 were excluded from the fit due to suspected problems of calibration.

Table 6. Chandra/HETG line fluxes of λ And[a]

Ion	$\lambda_{\rm model}$	log $T_{\rm max}$	$F_{\rm obs}$	S/N	ratio	Blends
Ar xvii	3.9491	7.3	2.09e-14	3.9	0.00	
S xvi	3.9908	7.4	9.47e-15	2.7	-0.13	S xvi 3.9920, Ar xvii 3.9941, 3.9942, S xv 3.9980
S xvi	4.7274	7.4	1.84e-14	3.7	-0.09	S xvi 4.7328
S xv	5.0387	7.2	4.05e-14	5.5	-0.05	
S xv	5.0665	7.1	1.87e-14	3.7	0.23	S xv 5.0631
S xv	5.1015	7.2	2.37e-14	4.2	0.06	S xv 5.0983, 5.1025
Si xiv	5.2168	7.2	2.27e-14	3.9	0.01	Si xiv 5.2180
Si xiv	6.1804	7.2	1.47e-13	20.4	0.01	Si xiv 6.1858
Mg xii	6.5800	7.0	4.39e-15	4.2	-0.23	Fe xxiv 6.5772, Mg xii 6.5802
Si xiii	6.6479	7.0	1.87e-13	25.7	-0.02	
Si xiii	6.6882	7.0	3.16e-14	10.5	-0.07	Si xiii 6.6850
No id.	6.7120	...	2.42e-15	3.3	...	
Si xiii	6.7403	7.0	1.23e-13	21.6	0.08	Mg xii 6.7378, Si xiii 6.7432
Mg xii	7.1058	7.0	4.53e-14	14.1	0.01	Mg xii 7.1069
Al xiii	7.1710	7.1	3.22e-14	12.0	-0.01	Fe xxiv 7.1690, Al xiii 7.1764
Mg xi	7.4730	6.8	1.07e-14	7.0	0.04	
Al xii	7.7573	6.9	3.04e-14	11.4	0.22	
Mg xi	7.8503	6.8	2.94e-14	11.4	0.01	
Al xii	7.8721	6.9	1.04e-14	6.7	-0.12	Al xii 7.8721
Fe xxiv	7.9857	7.3	1.56e-14	8.7	0.11	Fe xxiv 7.9960
Fe xxiii	8.3038	7.2	8.09e-15	6.3	-0.14	
Fe xxiv	8.3761	7.3	5.79e-15	5.3	0.17	Fe xx 8.3641
Mg xii	8.4192	7.0	3.33e-13	40.2	0.06	Mg xii 8.4246
Fe xxi	8.5740	7.1	8.48e-15	5.6	-0.01	
Fe xxii	8.9748	7.1	1.21e-14	6.9	-0.06	
Ni xxvi	9.0603	7.4	1.33e-14	7.7	-0.02	Fe xxii 9.0614, Fe xx 9.0647, 9.0659, 9.0683
No id.	9.1300	...	1.15e-14	7.1	...	
Mg xi	9.1687	6.8	2.03e-13	30.0	0.02	
Fe xxi	9.1944	7.1	1.69e-14	8.6	0.15	Fe xx 9.1882, 9.1979, Mg xi 9.1927, 9.1938
No id.	9.2190	...	6.70e-15	5.4	...	Ne x 9.215
Mg xi	9.2312	6.8	3.27e-14	12.0	-0.03	Mg xi 9.2282
Ni xix	9.2540	6.9	7.45e-15	5.7	0.29	
No id.	9.2870	...	1.40e-14	7.8	...	Ne x 9.291
Mg xi	9.3143	6.8	9.75e-14	20.6	0.09	
No id.	9.3600	...	1.16e-14	7.1	...	
Ni xx	9.3850	7.0	4.18e-15	4.2	-0.29	Ni xxvi 9.3853, Ni xxv 9.3900, Fe xxii 9.3933
Fe xxi	9.4797	7.0	3.71e-14	12.6	-0.08	Ne x 9.4807, 9.4809
Fe xix	9.6937	6.9	1.75e-14	8.5	0.42	Fe xix 9.6938
Ne x	9.7080	6.8	5.33e-14	14.8	-0.06	Fe xix 9.6938, Ne x 9.7085
Ni xix	9.9770	6.9	2.34e-14	9.6	-0.37	Ni xxv 9.9700, Fe xxi 9.9887, Fe xx 9.9977, 10.0004, 10.0054
No id.	10.0200	...	1.89e-14	8.6	...	Na xi 10.0232, 10.0286
Fe xx	10.0529	7.0	1.16e-14	6.7	0.03	
Fe xx	10.1203	7.0	1.31e-14	7.1	-0.18	Ni xix 10.1100, Fe xix 10.1195, Fe xvii 10.1210
Ne x	10.2385	6.8	1.91e-13	26.9	0.12	Ne x 10.2396
Fe xxiv	10.6190	7.3	3.43e-14	11.0	-0.16	Fe xix 10.6295
Fe xix	10.6491	6.9	1.34e-14	6.8	-0.22	Fe xix 10.6414
Fe xxiv	10.6630	7.3	2.28e-14	8.9	-0.14	Fe xvii 10.6570
Fe xvii	10.7700	6.8	1.32e-14	6.7	-0.25	Ne ix 10.7650, Fe xix 10.7650
Fe xix	10.8160	6.9	2.17e-14	8.6	0.01	
Fe xxiii	10.9810	7.2	3.23e-14	10.3	-0.16	
Ne ix	11.0010	6.6	1.55e-14	7.1	-0.03	Ni xxii 10.9920, 10.9927, Fe xix 11.0022
Fe xxiv	11.0290	7.3	4.17e-14	11.7	-0.20	Fe xxiii 11.0190, Fe xvii 11.0260
No id.	11.1000	...	6.16e-15	4.4	...	
Fe xvii	11.1310	6.8	1.20e-14	6.2	-0.28	Fe xxii 11.1376
Fe xxiv	11.1760	7.3	3.96e-14	11.1	-0.17	Fe xxiv 11.1870
Fe xvii	11.2540	6.8	1.89e-14	7.6	-0.35	Fe xxiv 11.2680
Ni xxii	11.3049	7.1	9.47e-15	5.4	-0.16	Fe xviii 11.2930, Fe xix 11.2980, Ni xxi 11.3180
Fe xviii	11.3260	6.9	2.64e-14	8.9	-0.13	Fe xxiii 11.3360
Fe xviii	11.4230	6.9	2.48e-14	8.4	-0.24	Fe xxii 11.4270
Fe xxiv	11.4320	7.3	2.79e-14	8.9	-0.00	
Fe xxiii	11.4580	7.2	1.08e-14	5.6	0.06	
Fe xxii	11.4900	7.1	1.30e-14	6.1	-0.19	
Fe xviii	11.5270	6.9	2.62e-14	8.4	-0.06	
Ne ix	11.5440	6.6	3.90e-14	10.2	0.01	Fe xviii 11.5740
Fe xxiii	11.7360	7.2	6.52e-14	12.9	-0.16	
Fe xxii	11.7700	7.1	6.53e-14	13.2	-0.19	
Fe xxii	11.8020	7.1	1.94e-14	7.2	0.28	
Ni xx	11.8320	7.0	1.69e-14	6.7	0.08	
Fe xxii	11.9320	7.1	2.00e-14	7.3	0.07	
Fe xxii	11.9770	7.1	2.44e-14	8.0	-0.11	Fe xxi 11.9750
Ne x	12.1321	6.8	8.32e-13	45.9	-0.06	Fe xvii 12.1240, Ne x 12.1375
Fe xxiii	12.1610	7.2	2.79e-14	8.4	-0.26	
Fe xxii	12.2100	7.1	2.48e-14	7.9	0.18	
Fe xvii	12.2660	6.8	6.12e-14	12.3	-0.03	
Fe xxi	12.2840	7.0	1.60e-13	19.8	0.01	
Fe xxi	12.3930	7.0	3.89e-14	9.7	0.11	Fe xxi 12.3940
Ni xix	12.4350	6.9	4.83e-14	10.7	-0.34	Fe xxi 12.4220, Fe xxii 12.4311, 12.4318
Fe xx	12.4680	7.0	1.52e-14	6.0	0.26	Fe xxi 12.4687
Fe xxi	12.4990	7.0	4.18e-14	9.9	0.21	Fe xxi 12.4956
Fe xxii	12.7540	7.1	3.33e-14	8.6	-0.04	
No id.	12.8100	...	6.88e-14	12.3	...	
Fe xx	12.8240	7.0	1.66e-13	19.0	-0.29	Fe xxi 12.8220, Fe xx 12.8460, 12.8640

Table 6. (cont). Chandra/HETG line fluxes of λ And[a]

Ion	$\lambda_{\rm model}$	log $T_{\rm max}$	$F_{\rm obs}$	S/N	ratio	Blends
Fe xx	12.9650	7.0	9.34e-14	14.1	-0.10	Fe xx 12.9120, Fe xix 12.9311, 12.9330, Fe xxii 12.9530
Fe xx	12.9920	7.0	1.56e-14	5.7	-0.19	
Fe xix	13.0220	6.9	3.26e-14	8.2	0.05	Fe xx 13.0240
Fe xx	13.0610	7.0	3.61e-14	8.7	0.01	Fe xx 13.0580
Fe xx	13.1000	7.0	1.35e-14	5.2	-0.05	
Fe xx	13.1530	7.0	4.54e-14	9.6	-0.09	Fe xx 13.1370
Fe xx	13.2740	7.0	5.72e-14	10.6	0.05	Fe xx 13.2240, 13.2241, Fe xxii 13.2360, Fe xxi 13.2487, Ni xx 13.2560, Fe xix 13.2658
Ni xx	13.3090	6.9	3.99e-14	8.8	0.04	Fe xx 13.3017, 13.3089, Fe xix 13.3191, Fe xviii 13.3230, Ni xx 13.3236
Fe xx	13.3850	7.0	4.82e-14	9.6	0.03	Fe xviii 13.3550, 13.3948
Fe xx	13.4090	7.0	2.51e-14	6.9	0.27	Fe xviii 13.4070
Fe xix	13.4230	6.9	4.01e-14	8.7	0.19	Fe xx 13.4181, Fe xxi 13.4308
Ne ix	13.4473	6.6	2.84e-13	23.2	0.02	Fe xix 13.4620
Fe xxi	13.5070	7.0	9.92e-14	13.6	0.04	Fe xix 13.4970
Fe xix	13.5180	6.9	9.04e-14	13.0	-0.14	
Fe xx	13.5350	7.0	3.75e-14	8.3	0.28	
Ne ix	13.5531	6.6	3.67e-14	8.2	-0.13	Fe xix 13.5510, 13.5540, Fe xx 13.5583
Fe xix	13.6450	6.9	3.83e-14	8.1	0.18	Fe xix 13.6481
Fe xix	13.6828	6.9	5.86e-14	10.1	0.35	Fe xix 13.6742, 13.6752, 13.6881, 13.6897
Ne ix	13.6990	6.6	1.10e-13	13.8	0.06	
Fe xix	13.7950	6.9	1.35e-13	15.2	-0.08	Fe xix 13.7315, 13.7458, 13.7590, Fe xx 13.7670, Ni xix 13.7790
Fe xvii	13.8250	6.8	4.80e-14	9.0	0.02	
Fe xix	13.8390	6.9	1.72e-14	5.4	-0.14	Fe xx 13.8430
Fe xviii	13.9530	6.9	2.93e-14	6.7	-0.08	Fe xix 13.9549, 13.9551, Fe xx 13.9620
Fe xxi	14.0080	7.0	2.52e-14	6.5	0.00	
Ni xix	14.0430	6.8	5.85e-14	9.8	0.24	
Ni xix	14.0770	6.8	3.17e-14	7.2	0.02	
Fe xviii	14.2080	6.9	1.80e-13	16.9	-0.18	
Fe xviii	14.2560	6.9	8.16e-14	10.7	-0.04	Fe xx 14.2670
Fe xviii	14.3430	6.9	1.89e-14	4.8	-0.29	
Fe xviii	14.3730	6.9	6.08e-14	8.5	-0.05	
Fe xviii	14.5340	6.9	5.80e-14	8.4	0.06	
Fe xviii	14.5710	6.9	7.69e-15	3.1	-0.54	Fe xx 14.5617
Fe xviii	14.6011	6.8	1.23e-14	3.8	-0.04	Fe xviii 14.6006
Fe xix	14.6640	6.9	4.63e-14	7.6	0.11	
Fe xix	14.7250	6.9	1.93e-14	5.1	-0.05	Fe xviii 14.7260
Fe xx	14.7540	7.0	2.21e-14	5.7	0.02	
O viii	14.8205	6.5	3.51e-14	7.6	0.20	
Fe xx	14.9703	7.0	3.77e-14	8.1	0.11	Fe xix 14.9610
Fe xvii	15.0140	6.7	2.95e-13	22.5	-0.26	
Fe xx	15.0470	7.0	2.25e-14	6.2	0.27	
Fe xix	15.0790	6.9	6.87e-14	10.8	0.23	
O viii	15.1760	6.5	6.76e-14	10.6	-0.08	O viii 15.1765, Fe xix 15.1770
Fe xix	15.1980	6.9	5.37e-14	9.5	0.20	
Fe xvii	15.2610	6.7	1.33e-13	14.8	-0.07	
Fe xvii	15.4530	6.7	2.93e-14	6.8	0.23	
Fe xviii	15.6250	6.8	7.00e-14	10.4	0.03	
Fe xviii	15.8240	6.8	5.04e-14	8.7	0.11	
Fe xviii	15.8700	6.8	4.68e-14	8.3	0.32	
O viii	16.0055	6.5	2.37e-13	18.6	-0.11	Fe xviii 16.0040, O viii 16.0067
Fe xviii	16.0710	6.8	1.54e-13	14.9	0.25	
Fe xix	16.1100	6.9	4.77e-14	8.3	-0.01	Fe xviii 16.1127
Fe xviii	16.1590	6.8	1.52e-14	4.7	-0.37	
Fe xvii	16.2285	6.7	8.52e-15	3.5	0.24	
Fe xix	16.2830	6.9	8.24e-15	3.4	-0.28	Fe xviii 16.2882
Fe xviii	16.3200	6.8	1.75e-14	5.0	0.26	
Fe xvii	16.3500	6.7	1.57e-14	4.7	0.18	Fe xix 16.3414
Fe xvii	16.7800	6.7	1.74e-13	15.0	-0.12	
Fe xvii	17.0510	6.7	2.41e-13	17.4	-0.01	
Fe xvii	17.0960	6.7	2.25e-13	16.7	0.06	
Fe xviii	17.6230	6.8	4.68e-14	7.1	-0.08	
O vii	18.6270	6.3	1.01e-14	3.1	-0.31	Ar xvi 18.6240
Ca xviii	18.6910	6.9	7.87e-15	2.7	-0.00	
O viii	18.9671	6.5	1.00e-12	29.4	-0.09	O viii 18.9725
O vii	21.6015	6.3	1.30e-13	8.2	0.03	
O vii	21.8036	6.3	1.01e-14	2.2	-0.22	
O vii	22.0977	6.3	7.63e-14	5.7	0.05	Ca xvii 22.1140

[a] Line fluxes (in erg cm^{-2} s^{-1}) measured in Chandra/HETG λ And spectra. log $T_{\rm max}$ indicates the maximum temperature (K) of formation of the line (unweighted by the EMD). "Ratio" is the log($F_{\rm obs}/F_{\rm pred}$) of the line. Blends amounting to more than 5% of the total flux for each line are indicated.

Table 7. XMM/RGS line fluxes of V851 Cen[a]

Ion	$\lambda_{\rm model}$	log $T_{\rm max}$	$F_{\rm obs}$	S/N	ratio	Blends
Si xiii	6.6480	7.0	4.51e-14	3.1	-0.00	Si xiii 6.6882, 6.7403, Mg xii 6.7378
Mg xii	8.4192	7.0	9.90e-14	7.8	0.07	Mg xii 8.4246
Mg xi	9.1687	6.8	3.52e-14	4.8	-0.14	
Mg xi	9.2312	6.8	4.64e-14	4.1	0.10	Mg xi 9.3143, Ni xxv 9.3400
Fe xxi	9.4797	7.0	3.82e-14	4.2	0.27	Ne x 9.4807, 9.4809
Ne x	9.7080	6.8	2.29e-14	4.1	-0.20	Ne x 9.7085
No id.	10.0200	…	4.41e-14	3.0	…	Na xi 10.0232, 10.0286
Ne x	10.2385	6.8	8.14e-14	7.2	-0.06	Ne x 10.2396
Fe xxiv	10.6190	7.3	3.80e-14	3.2	0.02	Fe xix 10.6414, 10.6491, Fe xvii 10.6570, Fe xxiv 10.6630
Fe xvii	10.7700	6.8	3.44e-14	2.4	0.09	Ni xxiii 10.7214, 10.8491, Ne ix 10.7650, Fe xix 10.8160
Fe xxiii	11.0190	7.2	4.97e-14	3.2	-0.07	Fe xxiii 10.9810, Ne ix 11.0010, Fe xxiv 11.0290
Fe xxiv	11.1760	7.3	2.64e-14	4.8	-0.04	Fe xvii 11.1310, Fe xxiv 11.1870
Fe xvii	11.2540	6.8	3.45e-14	2.9	0.25	Ni xxii 11.2118, Fe xxiv 11.2680, Fe xxiii 11.2850, Ni xxi 11.2908
Fe xviii	11.4230	6.9	2.20e-14	2.2	-0.14	Fe xxii 11.4270, Fe xxiv 11.4320, Fe xxiii 11.4580
Fe xviii	11.5270	6.9	4.40e-14	3.8	0.03	Fe xxii 11.4900, Ni xix 11.5390, Ne ix 11.5440
Fe xxii	11.7700	7.1	8.27e-14	6.0	-0.01	Fe xxiii 11.7360
Ne x	12.1320	6.8	4.99e-13	5.9	0.12	Ne x 12.1321
Fe xxi	12.2840	7.0	3.64e-14	3.2	-0.18	Fe xvii 12.2660
Ni xix	12.4350	6.9	3.97e-14	3.5	-0.17	Fe xxi 12.3930, 12.4220, 12.4990
Fe xx	12.8240	7.0	5.31e-14	5.2	-0.13	Fe xxi 12.8220, Fe xx 12.8460, 12.8640
Fe xx	12.9650	7.0	4.00e-14	4.3	0.04	Fe xx 12.9120, 12.9920, 13.0240,Fe xix 12.9330, 13.0220, Fe xxii 12.9530
Ne ix	13.4473	6.6	2.01e-13	13.3	0.12	
Fe xix	13.5180	6.9	5.92e-14	6.9	-0.13	Fe xix 13.4970, Fe xxi 13.5070, Ne ix 13.5531
Ne ix	13.6990	6.6	8.12e-14	8.5	0.05	Fe xix 13.6450, 13.7315, 13.7458
Fe xix	13.7950	6.9	3.81e-14	4.2	-0.04	Fe xx 13.7670, Ni xix 13.7790, Fe xvii 13.8250
Fe xxi	14.0080	7.0	4.81e-14	5.7	0.07	Ni xix 14.0430, 14.0770
Fe xviii	14.2080	6.9	6.40e-14	6.6	-0.13	Fe xviii 14.2080, Fe xviii 14.2560, Fe xx 14.2670
Fe xviii	14.3730	6.9	3.16e-14	5.0	-0.15	Fe xx 14.3318, Fe xviii 14.3430, Fe xviii 14.3430, Fe xx 14.4207, Fe xviii 14.4250, Fe xviii 14.4392
Fe xviii	14.5340	6.9	4.32e-14	4.3	0.24	Fe xviii 14.4856, Fe xviii 14.5056, Fe xviii 14.5710, Fe xviii 14.6011
O viii	14.8205	6.5	3.01e-14	4.6	0.31	Fe xviii 14.7820, O viii 14.8207, Fe xx 14.8276
Fe xvii	15.0140	6.7	9.47e-14	10.6	-0.21	Fe xix 15.0790
O viii	15.1760	6.5	5.19e-14	9.0	0.18	O viii 15.1765, Fe xix 15.1980
Fe xvii	15.2610	6.7	2.78e-14	4.4	-0.11	
Fe xvii	15.4530	6.7	1.56e-14	3.8	0.25	Fe xix 15.4136, Fe xviii 15.4940, Fe xx 15.5170, Fe xviii 15.5199
Fe xviii	15.6250	6.8	2.62e-14	4.6	0.23	
Fe xviii	15.8700	6.8	2.02e-14	3.7	0.13	Fe xviii 15.8240
O viii	16.0066	6.5	1.16e-13	10.3	-0.07	Fe xviii 16.0040, O viii 16.0055, Fe xviii 16.0710, Fe xix 16.1100, Fe xviii 16.1590
Fe xvii	16.7800	6.7	3.85e-14	6.1	-0.15	
Fe xvii	17.0510	6.7	1.02e-13	7.3	-0.01	Fe xvii 17.0960
Fe xviii	17.6230	6.8	6.16e-15	1.7	-0.34	
O vii	18.6270	6.3	1.83e-14	4.0	0.03	Ca xviii 18.6910
O viii	18.9671	6.5	3.45e-13	27.5	-0.08	O viii 18.9725
Ca xvi	21.4500	6.7	3.57e-15	2.2	-0.02	Ca xvi 21.4410
O vii	21.6015	6.3	3.78e-14	4.2	-0.08	Ca xvi 21.6100
O vii	22.0977	6.3	1.39e-14	2.2	-0.26	Ca xvii 22.1140
Ar xvi	23.5460	6.7	6.92e-15	1.4	0.09	Ar xvi 23.5900, Ca xvi 23.6260
N vii	24.7792	6.3	3.26e-14	7.4	0.00	N vii 24.7846, Ar xvi 24.8540
Ar xvi	24.9910	6.7	4.30e-15	1.4	-0.08	Ar xvi 24.9910, Ar xvi 25.0130, Ar xv 25.0500
C vi	26.9896	6.2	2.70e-15	1.2	0.30	C vi 26.9901
C vi	28.4652	6.2	2.35e-15	1.8	-0.21	C vi 28.4663
C vi	33.7342	6.1	2.10e-14	4.6	-0.01	C vi 33.7396

[a] Line fluxes (in erg cm^{-2} s^{-1}) measured in XMM/RGS V851 Cen spectra. log $T_{\rm max}$ indicates the maximum temperature (K) of formation of the line (unweighted by the EMD). "Ratio" is the log($F_{\rm obs}/F_{\rm pred}$) of the line. Blends amounting to more than 5% of the total flux for each line are indicated.